Journal of Applied Physics ARTICLE scitation.org/journal/jap

Polyamorphism in a solute-lean Al–Ce metallic glass

Cite as: J. Appl. Phys. **129**, 025108 (2021); doi: 10.1063/5.0036328
Submitted: 4 November 2020 · Accepted: 23 December 2020 ·
Published Online: 12 January 2021

Ziliang Yin,[1] Hongbo Lou,[1,a)] Hongwei Sheng,[2] Zhidan Zeng,[1] Wendy L. Mao,[3,4] and Qiaoshi Zeng[1,5,a)]

AFFILIATIONS

[1]Center for High Pressure Science and Technology Advanced Research, Pudong, Shanghai 201203, People's Republic of China
[2]Department of Physics and Astronomy, George Mason University, Fairfax, Virginia 22030, USA
[3]Department of Geological Sciences, Stanford University, Stanford, California 94305, USA
[4]Stanford Institute for Materials and Energy Sciences, SLAC National Accelerator Laboratory, Menlo Park, California 94025, USA
[5]Jiangsu Key Laboratory of Advanced Metallic Materials, School of Materials Science and Engineering, Southeast University, Nanjing 211189, People's Republic of China

[a)]**Authors to whom correspondence should be addressed:** zengqs@hpstar.ac.cn and hongbo.lou@hpstar.ac.cn

ABSTRACT

Polyamorphism discovered in lanthanide-rich metallic glasses (MGs) has been attributed to the electronic transition of the lanthanide element as a solvent element. In this work, we report that pressure-induced polyamorphism still exists in a Ce-poor $Al_{93}Ce_7$ binary MG where the 4*f* electron element serves as a solute and solute–solute avoidance is expected. The polyamorphic transition, observed by *in situ* high-pressure synchrotron x-ray diffraction, is accompanied by a volume collapse of ~0.78% and occurs over a narrow pressure range from ~0.8 to ~1.8 GPa. Further synchrotron Ce L_3-edge x-ray absorption spectroscopy measurements reveal that pressure-induced 4*f* electron delocalization underlies the polyamorphic transition. Molecular dynamics simulations confirm that the Ce atoms in the MG are completely isolated by the solvent Al atoms. This result demonstrates that 4*f* element-bearing alloys with extremely dilute concentrations can also exhibit polyamorphic states originating from electronic transitions, extending the compositional space of polyamorphism of MGs into very dilute regions. Our work suggests that tunable properties under compressive stress could be achieved in MGs by even minor doping of elements prone to electronic transitions.

INTRODUCTION

Polymorphism is common in crystalline materials, referring to the existence of two or more phases with different crystal structures but identical compositions. Graphite and diamond are well-known examples of polymorphism. In contrast, the "polyamorphism" counterpart in amorphous materials is rather complicated and is not easily recognizable due to the high degree of disorder encountered, and thus it remains an intriguing but challenging topic in condensed matter physics. After decades of efforts, polyamorphic transitions (PTs) have been reported in various amorphous network materials with directional bonding and an open atomic structure, e.g., amorphous ice,[1,2] oxides,[3–6] chalcogenides,[7,8] silicon,[9] and germanium.[10] The PTs in these systems typically exhibit noticeable density changes between a relatively low-density amorphous state (LDAS) and a relatively high-density amorphous state (HDAS), which may be attributed to an increase in the atomic coordination number and a collapse of the open atomic structure into a denser atomic-packing structure under high pressure. As a new class of amorphous solids, metallic glasses feature non-directional metallic bonding and are densely packed with a maximum number of nearest neighbors; therefore, similar PTs were thought to be improbable in MGs.

However, PTs were surprisingly discovered in a $Ce_{55}Al_{45}$ MG[11] ribbon and a $La_{32}Ce_{32}Al_{16}Ni_5Cu_{15}$ bulk metallic glass (BMG)[12] under compression. Zeng *et al.*[13] were able to verify by *in situ* Ce L_3-edge synchrotron x-ray absorption spectroscopy (XAS) that the origin of the pressure-induced polyamorphism in Ce-based MG could be attributed to delocalization of 4*f* electrons in Ce atoms under high pressure, and that the behavior of Ce-based MG resembles the electronic transitions in pure crystalline Ce. Later on, Li *et al.*[14] systematically investigated a few lanthanide-based MGs and proposed that the

origin of the PTs is a result of inheritance of the electronic structure of lanthanide-solvent atoms from their crystalline counterparts. This scenario was supported by many subsequent studies in lanthanide-based MGs[15–19] and also is in line with another argument in MGs that solvent elements dictate the properties of MGs.[20,21] However, the lanthanide-solvent atoms originated polyamorphism is inconsistent with the observation in crystalline $Ce_{88}Pr_{12}$ alloys, which could show two separate volume collapse transitions inherited from pure Ce and Pr, respectively.[22] Recently, a pressure-induced PT was observed in a $La_{43.4}Pr_{18.6}Al_{14}Cu_{24}$ MG.[23] Since La does not contain 4*f* electrons and no pressure-induced PT was reported in La-based MGs,[24] the polyamorphism found in the $La_{43.4}Pr_{18.6}Al_{14}Cu_{24}$ MG may well be attributed to Pr atoms with an electron configuration of [Xe] $4f^3 6s^2$ despite the fact that Pr is a solute with a relatively low atomic concentration. In another work, a PT was absent in $Mg_{65}Cu_{25}Tb_{10}$ BMG, which possesses a 4*f* electron element, Tb, as the solute element, up to 31.19 GPa.[25] Therefore, it is still in question whether polyamorphism exists in MGs with 4*f* electron elements serving as the solute. In other words, would the transition of the electronic structure of pure lanthanide elements still be inherited in MGs with a very low concentration such that all lanthanide atoms are completely isolated from one another by other atoms without 4*f* electrons?

In this paper, we chose a binary $Al_{93}Ce_7$ MG with a very low Ce concentration (all the solute Ce atoms are expected to be isolated by the solvent Al atoms) and studied its atomic and electronic structural evolution *in situ* under pressure by high-pressure x-ray diffraction (XRD), *in situ* high-pressure Ce L_3-edge XAS, and molecular dynamics (MD) simulations. Even at very low solute concentration, we demonstrate that PTs still occur in lanthanide-solute MGs via the same mechanism of 4*f* electronic transition in the lanthanide elements under high pressure.

EXPERIMENTAL

$Al_{93}Ce_7$ MG ribbons with a thickness of ~20 μm and a width of about ~1 mm were prepared by single-roller melt spinning. Master ingots with the nominal composition were prepared by arc-melting a mixture of high purity Ce (99.9 at. %) and Al (99.99 at. %) in a zirconium-gettered high-purity argon atmosphere. The amorphous nature of the prepared samples was confirmed by XRD and differential scanning calorimetry (DSC). *In situ* high-pressure angle-dispersive XRD experiments with an x-ray wavelength of 0.4959 Å and a focused x-ray beam size of $\sim 10 \times 10\ \mu m^2$ were carried out on the $Al_{93}Ce_7$ MG at the beamline 12.2.2, Advanced Light Source (ALS), Lawrence Berkeley National Laboratory (LBNL). A symmetric diamond anvil cell (DAC) with an anvil culet size of 500 μm was used to generate high pressure. The gasket was T301 stainless steel gasket. A 4:1 methanol–ethanol mixture (volume ratio) was used as the pressure-transmitting medium, which provides nearly hydrostatic pressure conditions below 10 GPa.[26] The pressure was determined by the ruby fluorescence method.[27]

In situ high-pressure Ce L_3-edge XAS experiments were carried out on $Al_{93}Ce_7$ MG at the beamline 20-BMB, Advanced Photon Source (APS), Argonne National Laboratory (ANL). The x-ray beam size was $\sim 12 \times 6\ \mu m^2$. A panoramic DAC with a diamond anvil culet of ~300 μm was employed to provide a large opening perpendicular to the compression axis. The ribbon samples were cut into squares with sizes of $\sim 70 \times 70 \times 20\ \mu m^3$, and then two pieces of square samples were loaded in the panoramic DAC and piled up to reach an optimized sample thickness of ~40 μm (one attenuation length is ~35 μm at 5.723 keV) for the Ce L_3-edge XAS experiment. A transmission mode was used with ion chambers filled with an Ar–N_2 (volume ratio, 1:9) gas mixture as incident and transmitted photon detectors. The DAC was tilted by ~7° to minimize photon absorption of the Be gasket and diamond anvils and also to avoid strong diffraction generated by the single-crystal diamond anvils. The sample deliberately leant against the sample chamber wall. Therefore, the x-ray beam went through an x-ray transparent Be gasket and could have an optimized sample thickness close to 40 μm on the beam path. The x-ray energy was calibrated by a Cr foil located at the downstream end of the beam path. The pressure was also determined by ruby fluorescence from tiny ruby balls loaded along the sample in the DAC.

Classical MD simulations were carried out on $Al_{93}Ce_7$ MG with a total of 32 000 atoms. Two interatomic potentials for Al–Ce were developed to simulate the two amorphous states, representing the interactions of Al with *f*-localized Ce (trivalent) and Al with *f*-delocalized Ce (tetravalent), respectively. The trivalent and tetravalent valence states of Ce correspond to the LDAS and the HDAS established by the 4*f*-electron localization/delocalization hypothesis. This approach has been successfully used to investigate the structure ordering induced by pressure in Ce–Al MGs.[11,28] More details of the MD simulations can be found in Ref. 28. Following the classical MD simulation of the 256-atom MGs, the as-obtained MG structures were further equilibrated in an NPT (constant number of particles, pressure, and temperature) ensemble (300 K) with a density functional theory (DFT)-based Vienna *Ab-initio* Simulation Package (VASP).[29] For the *ab initio* MD simulation, the projector augmented-wave (PAW) method[30,31] was adopted to describe the electron–ion interactions and the generalized gradient approximation (GGA) for the exchange correlation functions. The valence electrons of Al were specified as $3s^2 3p^1$. For Ce, the 4*f* electrons were treated as either the localized state (trivalent, $5s^2 5p^6 6s^2 5d^1 4f^0$) or the itinerant state (tetravalent, $5s^2 5p^6 6s^2 5d^1 4f^1$) including semi-core states, respectively.

RESULTS AND DISCUSSION

Figure 1 shows the XRD patterns of $Al_{93}Ce_7$ MG collected during compression at room temperature. The ambient pressure data were collected outside the DAC, and the starting pressure inside the DAC was 0.3 GPa. Only a principal diffraction peak (PDP) around 2.6 $Å^{-1}$ and a pre-peak around 1.2 $Å^{-1}$ from $Al_{93}Ce_7$ MG can be observed, indicating that the sample remains fully amorphous over the entire pressure range up to 8.7 GPa. Since the structural origin of the pre-peak remains elusive in glasses, following previous studies, we only focus on the PDP in this work. The position of the PDP, Q_1, obtained from a Voigt fit, shifts to a higher Q range with increasing pressure as expected from the densification effect. Q_1 is related to the atomic volume in MG systems following a power–law relationship.[32,33] In this work, the 2.5 power–law[34–36] that was experimentally verified to relate Q_1 with volume under pressure in MGs was adopted to estimate the volume changes during compression.

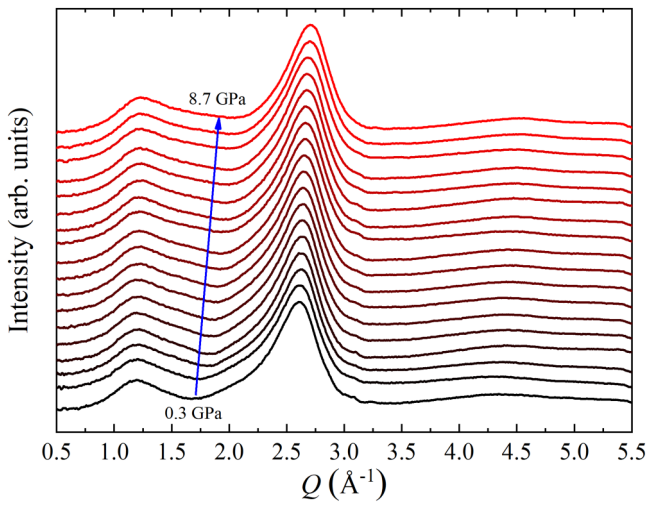

FIG. 1. *In situ* high-pressure synchrotron XRD patterns of $Al_{93}Ce_7$ MG from 0.3 to 8.7 GPa at room temperature.

Figure 2 shows the relative volume, $V_P/V_0 = (Q_{1\_0}/Q_{1\_P})^{2,5}$ (where the subscripts *0* and *P* denote the initial-pressure and a given pressure, respectively), of $Al_{93}Ce_7$ MG as a function of pressure. In Fig. 2(a), a second-order Birch–Murnaghan equation of state (BM-EOS) was used to fit the data over the entire pressure range. However, a single BM-EOS was found to poorly describe the entire dataset. Instead, as shown in Fig. 2(b), the data above ~1.8 GPa or below ~0.8 GPa can be fit well by a single BM-EOS, which suggests two distinct amorphous states below ~0.8 GPa and above ~1.8 GPa and a polyamorphic transition in between. A volume collapse of ~0.78% between the two different states at ambient pressure can be resolved, indicating a pressure-induced PT in the dilute Ce-bearing $Al_{93}Ce_7$ MG. When the pressure is fully released to 0 GPa, the PDP position, Q_1, returns to the initial value before compression, which indicates that the pressure-induced PT process is reversible in $Al_{93}Ce_7$ MG [as shown in Fig. 2(b)].

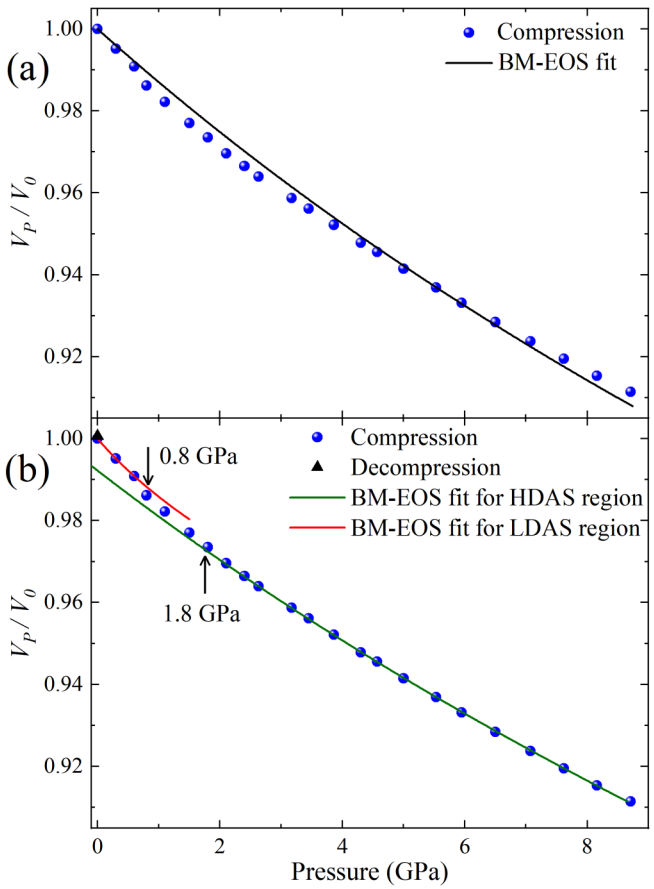

FIG. 2. The relative volume change V_P/V_0 of $Al_{93}Ce_7$ MG as a function of pressure. (a) The black line represents the single BM-EOS fit for the entire pressure region. (b) The red and green lines show the BM-EOS fits for the LDAS region (below ~0.8 GPa) and HDAS region (above ~1.8 GPa), respectively. The solid black triangle represents the data after pressure is fully released. The error bars for the experimental data are smaller than the symbol size.

For Ce-based MGs, the mechanism of PTs can be traced back to pure, crystalline cerium, which undergoes a face-centered cubic isostructural γ-α phase transition at ~0.9 GPa with a sharp volume collapse of ~15% caused by the delocalization of the 4*f* electrons.[37] Likewise, in two lanthanide-solvent MG systems, $Ce_{75}Al_{25}$ MG[13] and $Ce_{60}Al_{20}Co_{20}$ BMG,[38] the delocalization of the 4*f* electrons was experimentally observed during their PTs. It is intriguing to verify whether the PT observed in the highly dilute lanthanide-solute $Al_{93}Ce_7$ MG is still linked with the 4*f* electron delocalization mechanism. To address this question, *in situ* high-pressure Ce L_3-edge XAS experiments were carried out on $Al_{93}Ce_7$ MG, and the XAS spectra as a function of pressure are shown in Fig. 3. At ambient conditions, the spectrum shows a pure $4f^1$ component and represents a completely localized 4*f* electronic state. During compression, a peak appears at energy ~10 eV higher than the characteristic $4f^1$ peak, which represents the appearance of $4f^0$ electrons, a delocalized state. The intensity of the $4f^0$ component grows with increasing pressure at the expense of the intensity of the $4f^1$ component. The transfer of spectra weight from the $4f^1$ to the $4f^0$ component provides direct experimental evidence for 4*f* electron delocalization in the lanthanide-solute $Al_{93}Ce_7$ MG under high pressure. This spectroscopic evidence showing the delocalization of 4*f* electrons is in agreement with what we previously demonstrated in the PTs of Ce-based MGs.[8] The delocalization of 4*f* electrons was observed to occur at ~1.0 GPa as shown in Fig. 3, which coincides with the volume collapse of $Al_{93}Ce_7$ MG in the pressure range from ~0.8 to ~1.8 GPa, corroborating that the PT in this alloy is closely related to the delocalization of 4*f* electrons when Ce is the solute element (i.e., Ce-poor compositions).

To further analyze the structural characteristics of $Al_{93}Ce_7$ MG at the atomic level, classical MD simulations were carried out. Our primary goal was to examine the structural differences of the two amorphous states of $Al_{93}Ce_7$ MG. This approach has been

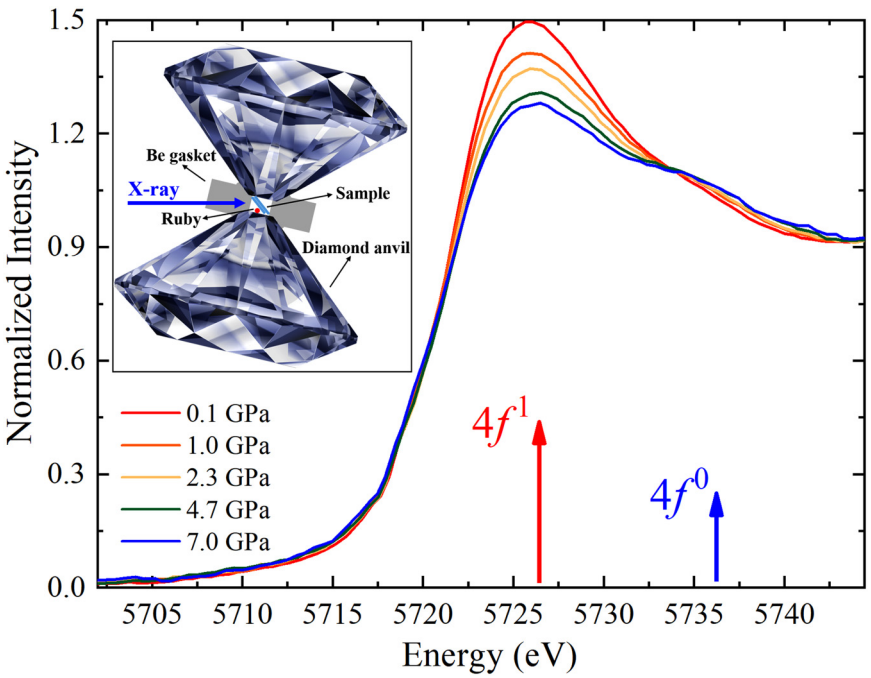

FIG. 3. *In situ* high-pressure Ce L_3-edge XAS spectra of $Al_{93}Ce_7$ MG as a function of pressure. The arrows indicate the $4f^0$ and $4f^1$ components. The inset is a schematic illustration of *in situ* high-pressure XAS experimental geometry.

previously employed to investigate the pressure-induced structural changes in Ce–Al MGs.[11,28] The pair distribution functions (PDFs) for the two amorphous states of $Al_{93}Ce_7$ MG at ambient conditions are shown in Fig. 4. The PDFs of $Al_{93}Ce_7$ MG at two different amorphous states are very similar. The most noticeable difference is the shoulder of the first peak around ~3.3 Å. The inset of Fig. 4 shows the partial PDF of the two states. It can be seen that the first peak of Ce–Ce partial PDF appears at ~6 Å, which indicates there

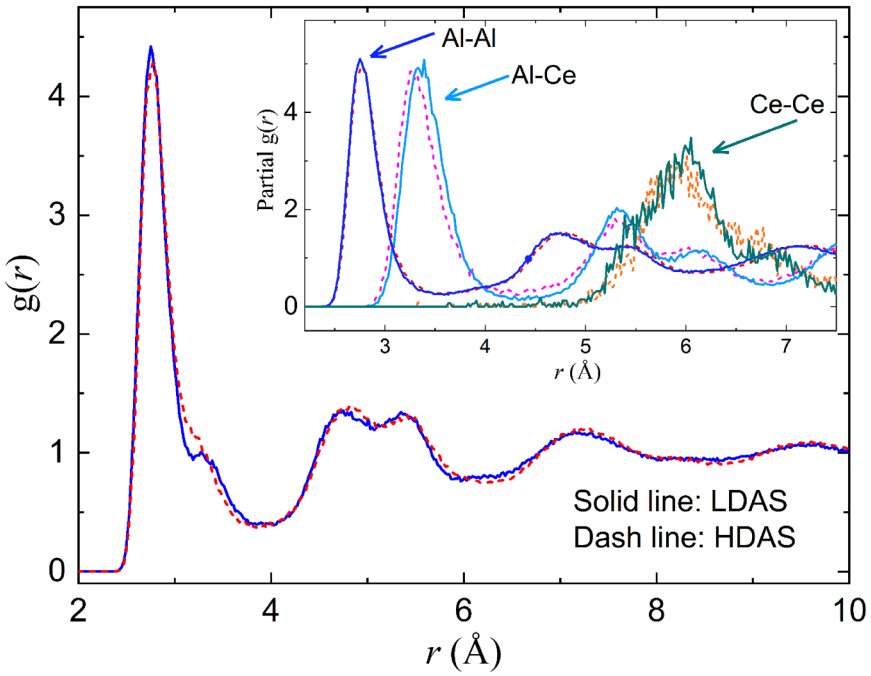

FIG. 4. PDFs for the LDAS and HDAS of $Al_{93}Ce_7$ MG at room temperature; inset shows the partial PDF. The solid and dashed lines represent the LDAS and the HDAS, respectively.

is almost no Ce–Ce direct bonding contribution in the nearest neighbor shell in $Al_{93}Ce_7$ MG, indicating the phenomenon of solute–solute avoidance in the MG. This also verifies our assumption that Ce atoms are totally isolated solute atoms and coordinated by Al atoms in the first atomic shell. The shoulder around ~3.3 Å in the total PDF is contributed by the Al–Ce, which is, indeed, influenced most significantly by the Ce 4*f* electron delocalization since Ce atoms are directly bonded with Al atoms only in the system. The Al–Al partial PDF is almost unchanged, which further confirms that the PT observed in the $Al_{93}Ce_7$ MG is due to a configuration change in the Ce atom. Our *ab initio* MD simulation of the two amorphous states of $Al_{93}Ce_7$ further confirms a small density difference (~2.8%) of the MG before and after *f*-electron delocalization (at 0 K and 0 GPa, the volume of the 4*f*-localized and 4*f*-delocalized $Al_{93}Ce_7$ is 18.5141 $Å^3$ per atom and 17.9975 $Å^3$ per atom, respectively), which is close to the small volume collapse of ~1% in our experimental estimation giving experimental uncertainty and different processing conditions between experiments and simulations.

The delocalization of 4*f* electrons in the Ce atoms accounts for the polymorphic phase transition and volume collapse in $Al_{93}Ce_7$ MG, $Ce_{75}Al_{25}$ MG, and pure crystalline Ce. The pressure-induced 4*f*-electron delocalization enhances the electronic bonding and decreases the Ce radius, resulting in a volume collapse in Ce-bearing MG systems.[11] Ce also plays a larger role in the volume reduction of the Ce–Al system under pressure since the bulk modulus of Al (~76 GPa) is much larger than that of Ce (~22 GPa).

In $Al_{93}Ce_7$ MG, the low concentration of 7% of Ce should be the reason why the volume collapse of $Al_{93}Ce_7$ MG is only ~0.78%, which seems to simply scale with the concentration of Ce given ~8.6% reported in $Ce_{75}Al_{25}$ MG.[13] The specific atomic packing structure in $Al_{93}Ce_7$ MG also explains the differences in the width of the transition region for different compositions. Ce atoms have identical environments in pure Ce metal; thus, the isostructural γ–α phase transition occurs abruptly at ~0.9 GPa. By alloying 25% Al atoms in the Ce solvent, the environment around Ce atoms becomes more complicated in $Ce_{75}Al_{25}$ MG, resulting in a wider transition region from ~1.5 GPa to ~5 GPa.[13] While in $Ce_{55}Al_{45}$ MG, there are even more packing complexities than in $Ce_{75}Al_{25}$ MG, the transition region of 2–13.5 GPa[11] is the widest among all the reported Ce–Al binary systems. In this work, the Ce concentration in $Al_{93}Ce_7$ MG is extremely low, and the solute Ce atoms are confirmed to be isolated by the solvent Al atoms. This renders a relatively uniform atomic environment around Ce atoms, and consequently, the transition region is quite sharp from ~0.8 to ~1.8 GPa. For the simple Ce–Al binary system, one may argue that the larger the difference between the concentration of Ce (C_{Ce}) and Al (C_{Al}) is, the simpler the Ce atomic environment. Thus, the width of the transition range is inversely proportional to $|C_{Ce}\text{-}C_{Al}|$ rather than the C_{Ce} previously proposed in Ce-based MGs.[39]

For multicomponent systems, the local structure becomes even more complicated, as does the chemical interactions. For instance, when a small concentration of Al in $Ce_{75}Al_{25}$ MG is replaced by a covalent element, Si, to form $Ce_{75}Al_{23}Si_2$ MG, the transition pressure changes, and the transition pressure range is twice as large as that of the parent alloy.[40] The addition of foreign atoms introduces more chemical and topological complexities into the MGs and has a pronounced impact on the kinetics of the PTs. Therefore, the absence of a polyamorphic transition in $Mg_{65}Cu_{25}Tb_{10}$ BMG[25] may not be caused by the relatively lower 4*f*-element concentration than that in the $La_{43.4}Pr_{18.6}Al_{14}Cu_{24}$ MG,[23] but is rather due to two reasons. First, the low concentration of *f*-electron bearing element, Tb, could only lead to a small volume collapse that necessitates careful experimental inspections with small pressure steps. Second, the dilute Tb atoms in the ternary alloy system have diverse local atomic environments, resulting in a relatively large pressure range for the transition. It would be difficult to observe a small volume change over a wide pressure range with large pressure intervals adopted in Ref. 25. In the current work, we used small pressure intervals of ~0.2 GPa and focused on the low-pressure range, which makes it possible to detect the small volume change in $Al_{93}Ce_7$ MG.

Although the atomic structure of MGs is still far from being completely understood, the packing of the solute-centered quasi-equivalent clusters model has been extensively used in recent years.[41,42] This model promotes the understanding of MGs' properties by atomic packing extended from the short-range order (SRO) to medium-range order (MRO). For a given glass system, the SRO is characterized by solute-centered quasi-equivalent clusters, each of which is composed of a solute atom surrounded by a large number of solvent atoms. The MRO can be regarded as the next-level structural organization beyond the SRO, which is considered to be formed in the cluster–cluster connection scheme.[42] For $Al_{93}Ce_7$ MG, the solute Ce atoms are surrounded by solvent Al atoms forming SROs; MROs form by connecting these SROs. When the pressure exceeds a certain value, the size of Ce atoms will decrease due to delocalization, and the volume of the Ce-centered clusters (SROs) and the higher-level MROs will also decrease accordingly, resulting in a global volume collapse. In the past, the focus has been on the dominant role of solvent atoms forming the framework of MGs. For example, Ma *et al.*[20] proposed that the mechanical properties and elastic moduli in BMGs are dominated by the solvents; Li *et al.*[14] suggested that polyamorphism in lanthanide-based MGs is inherited from its crystalline lanthanide-solvent constituent with pressure-induced delocalization of 4*f* electrons. Our results reveal that pressure-induced polyamorphism is possible in systems where dilute solute atoms play a key role, further pointing to the critical effects of minor alloying in MGs.[43,44]

SUMMARY

In conclusion, a lanthanide-solute MG, $Al_{93}Ce_7$, with an extremely low Ce concentration, was studied using *in situ* high-pressure synchrotron XRD, XAS, and MD simulations. A pressure-induced PT from LDAS to HDAS with a relatively narrow transition region of 0.8–1.8 GPa was observed, accompanied by a slight volume collapse of ~0.78%. The results from XAS demonstrate that PT in $Al_{93}Ce_7$ MG can be attributed to the delocalization of 4*f* electrons in the dilute lanthanide element. The MD simulation results confirm that the Ce atoms are isolated (real solute atoms both locally and globally) in the Al solvent. The relatively small transition range and volume collapse of $Al_{93}Ce_7$ MG are due to the low concentration of

Ce and the relatively similar local environment around the Ce atoms. These results demonstrate that electronic PTs can occur in dilute 4*f* element-bearing MGs. This work also reveals the highly tunable characteristics of the 4*f*-electron elements and suggests that the solute atoms could play essential roles in affecting the structure and properties of MGs. The findings expand the compositional space into very dilute regions and could provide new insights into the mechanism of polyamorphism. Moreover, these results also could shed new light on the long-sought minor alloying effect in MGs and may stimulate more studies using lanthanide-solute atoms as property-tuning knobs under compressive stress over a wide concentration range or as probe atoms for structural studies of MGs.

ACKNOWLEDGMENTS

This research was supported by the National Natural Science Foundation of China (NNSFC; Nos. 51871054 and U1930401) and the Fundamental Research Funds for the Central Universities. This research used the beamline 12.2.2 of the Advanced Light Source (ALS), a Department of Energy (DOE) Office of Science User Facility under Contract No. DE-AC02-05CH11231 and the beamline 20-BM-B of the Advanced Photon Source (APS), a U.S. Department of Energy (DOE) Office of Science User Facility operated for the DOE Office of Science by Argonne National Laboratory (ANL) under Contract No. DE-AC02-06CH11357. Beamline 20-BM-B operations are supported by the U.S. DOE and the Canadian Light Source. The authors thank Dr. C. J. Sun for his support of GUP experiment done at 20-BM-B beamline of APS.

DATA AVAILABILITY

The data that support the findings of this study are available from the corresponding author upon reasonable request.

REFERENCES

[1]C. A. Tulk, R. Hart, D. D. Klug, C. J. Benmore, and J. Neuefeind, Phys. Rev. Lett. **97**, 115503 (2006).
[2]O. Mishima and Y. Suzuki, Nature **419**, 599 (2002).
[3]J. P. Itie, A. Polian, G. Calas, J. Petiau, A. Fontaine, and H. Tolentino, Phys. Rev. Lett. **63**, 398 (1989).
[4]C. Meade, R. J. Hemley, and H. K. Mao, Phys. Rev. Lett. **69**, 1387 (1992).
[5]S. K. Lee, P. J. Eng, H. K. Mao, Y. Meng, and J. Shu, Phys. Rev. Lett. **98**, 105502 (2007).
[6]E. Soignard, S. A. Amin, Q. Mei, C. J. Benmore, and J. L. Yarger, Phys. Rev. B **77**, 144113 (2008).
[7]Q. Mei, C. J. Benmore, R. T. Hart, E. Bychkov, P. S. Salmon, C. D. Martin, F. M. Michel, S. M. Antao, P. J. Chupas, P. L. Lee, S. D. Shastri, J. B. Parise, K. Leinenweber, S. Amin, and J. L. Yarger, Phys. Rev. B **74**, 014203 (2006).
[8]W. A. Crichton, M. Mezouar, T. Grande, S. Stølen, and A. Grzechnik, Nature **414**, 622 (2001).
[9]P. F. McMillan, M. Wilson, D. Daisenberger, and D. Machon, Nat. Mater. **4**, 680 (2005).
[10]M. H. Bhat, V. Molinero, E. Soignard, V. C. Solomon, S. Sastry, J. L. Yarger, and C. A. Angell, Nature **448**, 787 (2007).
[11]H. W. Sheng, H. Z. Liu, Y. Q. Cheng, J. Wen, P. L. Lee, W. K. Luo, S. D. Shastri, and E. Ma, Nat. Mater. **6**, 192 (2007).
[12]Q. S. Zeng, Y. C. Li, C. M. Feng, P. Liermann, M. Somayazulu, G. Y. Shen, H. K. Mao, R. Yang, J. Liu, T. D. Hu, and J. Z. Jiang, Proc. Natl. Acad. Sci. U.S.A. **104**, 13565 (2007).
[13]Q. S. Zeng, Y. Ding, W. L. Mao, W. Yang, S. V. Sinogeikin, J. Shu, H. K. Mao, and J. Z. Jiang, Phys. Rev. Lett. **104**, 105702 (2010).
[14]G. Li, Y. Y. Wang, P. K. Liaw, Y. C. Li, and R. P. Liu, Phys. Rev. Lett. **109**, 125501 (2012).
[15]C. L. Lin, A. S. Ahmad, H. B. Lou, X. D. Wang, Q. P. Cao, Y. C. Li, J. Liu, T. D. Hu, D. X. Zhang, and J. Z. Jiang, J. Appl. Phys. **114**, 213516 (2013).
[16]Y. Y. Wang, W. Zhao, G. Li, Y. C. Li, and R. P. Liu, Mater. Lett. **110**, 184 (2013).
[17]W. Zhao, Y. Y. Wang, R. P. Liu, and G. Li, Appl. Phys. Lett. **102**, 031903 (2013).
[18]Y. Wang, X. Dong, X. Song, J. Wang, G. Li, and R. Liu, Mater. Lett. **162**, 203 (2016).
[19]Y. Y. Wang, X. Dong, X. Song, X. P. Li, and G. Li, Mater. Lett. **192**, 142 (2017).
[20]D. Ma, A. D. Stoica, X. L. Wang, Z. P. Lu, B. Clausen, and D. W. Brown, Phys. Rev. Lett. **108**, 085501 (2012).
[21]W. H. Wang, Prog. Mater. Sci. **57**, 487 (2012).
[22]C. S. Perreault, N. Velisavljevic, G. K. Samudrala, G. Kalai Selvan, and Y. K. Vohra, High Pressure Res. **38**, 270 (2018).
[23]L. Li, L. Wang, R. Li, D. Qu, H. Zhao, K. W. Chapman, P. J. Chupas, and H. Liu, Phys. Status Solidi RRL **11**, 1700078 (2017).
[24]H. W. Sheng, E. Ma, H. Z. Liu, and J. Wen, Appl. Phys. Lett. **88**, 171906 (2006).
[25]G. Li, Y. C. Li, Z. K. Jiang, T. Xu, L. Huang, J. Liu, T. Zhang, and R. P. Liu, J. Non-Cryst. Solids **355**, 521 (2009).
[26]R. J. Angel, M. Bujak, J. Zhao, G. D. Gatta, and S. D. Jacobsen, J. Appl. Crystallogr. **40**, 26 (2007).
[27]H. K. Mao, J. Xu, and P. M. Bell, J. Geophys. Res. Solid Earth **91**, 4673 (1986).
[28]Q. Zeng, H. Sheng, Y. Ding, L. Wang, W. Yang, J. Z. Jiang, W. L. Mao, and H. K. Mao, Science **332**, 1404 (2011).
[29]G. Kresse and J. Hafner, Phys. Rev. B **49**, 14251 (1994).
[30]P. E. Blöchl, Phys. Rev. B **50**, 17953 (1994).
[31]G. Kresse and D. Joubert, Phys. Rev. B **59**, 1758 (1999).
[32]A. R. Yavari, A. L. Moulec, A. Inoue, N. Nishiyama, N. Lupu, E. Matsubara, W. J. Botta, G. Vaughan, M. D. Michiel, and Å. Kvick, Acta Mater. **53**, 1611 (2005).
[33]D. Ma, A. D. Stoica, and X. L. Wang, Nat. Mater. **8**, 30 (2009).
[34]Q. Zeng, Y. Kono, Y. Lin, Z. Zeng, J. Wang, S. V. Sinogeikin, C. Park, Y. Meng, W. Yang, H. K. Mao, and W. L. Mao, Phys. Rev. Lett. **112**, 185502 (2014).
[35]D. Z. Chen, C. Y. Shi, Q. An, Q. Zeng, W. L. Mao, W. A. Goddard, and J. R. Greer, Science **349**, 1306 (2015).
[36]Q. Zeng, Y. Lin, Y. Liu, Z. Zeng, C. Y. Shi, B. Zhang, H. Lou, S. V. Sinogeikin, Y. Kono, C. Kenney-Benson, C. Park, W. Yang, W. Wang, H. Sheng, H. K. Mao, and W. L. Mao, Proc. Natl. Acad. Sci. U.S.A. **113**, 1714 (2016).
[37]P. Soderlind, Adv. Phys. **47**, 959 (1998).
[38]L. Belhadi, F. Decremps, S. Pascarelli, L. Cormier, Y. Le Godec, S. Gorsse, F. Baudelet, C. Marini, and G. Garbarino, Appl. Phys. Lett. **103**, 111905 (2013).
[39]M. J. Duarte, P. Bruna, E. Pineda, D. Crespo, G. Garbarino, R. Verbeni, K. Zhao, W. H. Wang, A. H. Romero, and J. Serrano, Phys. Rev. B **84**, 224116 (2011).
[40]Q. S. Zeng, Y. Z. Fang, H. B. Lou, Y. Gong, X. D. Wang, K. Yang, A. G. Li, S. Yan, C. Lathe, F. M. Wu, X. H. Yu, and J. Z. Jiang, J. Phys. Condens. Matter **22**, 375404 (2010).
[41]D. B. Miracle, Nat. Mater. **3**, 697 (2004).
[42]H. W. Sheng, W. K. Luo, F. M. Alamgir, J. M. Bai, and E. Ma, Nature **439**, 419 (2006).
[43]C. T. Liu and Z. P. Lu, Intermetallics **13**, 415 (2005).
[44]W. H. Wang, Prog. Mater Sci. **52**, 540 (2007).